A theoretical model for wave attenuation by vegetation considering current effects

Huiran Liu, Haiqi Fang, Pengzhi Lin*

State Key Laboratory of Hydraulics and Mountain River Engineering, Sichuan University, Chengdu 610065, China

*Corresponding author, E-mail address: cvelinpz@scu.edu.cn (P. Lin)

Abstract

A new theoretical model is derived to predict wave attenuation in vegetation domain under current influences. The model is derived based on energy conservation and the wave decaying rate is expressed as the function of current velocity, wave orbital velocity, and incident wave amplitude. Considering the current effect on changing wave group velocity, the theory predicts an asymmetric behaviors of wave decay in following and opposing currents, different from the earlier theory that predicts a symmetry decay behavior by ignoring current effect on wave group velocity. The new theory shows that the wave height has a reciprocal decay for weak current but an exponential decay for strong current. In addition, the theory shows that the decay rate depends on both incident wave height and current velocity when the current velocity is relatively small to wave orbital velocity, whereas it is independent of incident wave amplitude when the current is strong. All of these wave decaying characteristics predicted by the theory have been confirmed by the available experimental data and the numerical results from a 2D RANS model (NEWFLUME).

Keywords: Theoretical model; Wave attenuation; Group Velocity; Wave-current-vegetation interaction; Numerical simulation.

1. Introduction

Aquatic vegetation such as salt marsh and mangrove is widely distributed in coastal and estuarial areas. It interacts with waves, tidal currents, and storm surges. The presence of vegetation can reduce flow velocity, increase turbulence mixing and then affect sediment suspension and transport (López and García, 1998; Nepf and Ghisalberti, 2008). As a result, it

reduces coastal erosion and increases habitat and species diversity. Moreover, when waves propagate through the vegetation domain, the wave energy is dissipated, and the wave height decreases inside the domain. Thus, aquatic vegetation can protect the coastal area from storm surges and tsunamis (Augustin et al., 2009; Kobayashi et al., 1993; Mendez and Losada, 2004; Suzuki et al., 2012).

Many studies were conducted for wave attenuation by vegetation. Based on the concept of energy conservation, Dalrymple et al. (1984) first derived a theoretical model to predict linear wave variation and attenuation in an emerged, uniform, rigid vegetation domain (we name the model as Dalrymple 1984 model for easy reference in this study). The wave height follows reciprocal decay based on this theory. Mendez and Losada (2004) extended the Dalrymple 1984 model to predict irregular wave attenuation in vegetation. They found that the drag coefficient C_D calculated by the theoretical solution correlates better with the KC (Keulegan–Carpenter) number than the Re (Reynolds) number. Mei et al. (2011) established a multi-scale model to solve the infinite-length wave-vegetation interaction based on the linear wave theory. Subsequently, Liu et al. (2015) extended the theory to a finite-length domain. In the meantime, experimental studies were conducted for wave attenuation, flow field and turbulence characteristics. For example, Dubi and Tørum (1995) found that when the vegetation is submerged, an increase in the submergence ratio leads to a decrease in wave attenuation. Augustin et al. (2009) compared the wave attenuation by emerged and submerged vegetation and found that waves decay faster in emerged vegetation. Pujol and Nepf (2012) studied the interaction of focusing waves with vegetation and found that the turbulence kinetic energy (TKE) generated by the breaking waves dissipated faster when vegetation existed. Lou et al. (2018) studied the wave interacting with vertical varying density vegetation and analyzed the wave attenuation, flow field structure, and turbulence information. In addition, numerical studies were carried out based on different governing equations. Lin (2008) proposed a 2D porous media model NEWFLUME based on spatially-averaged Navier-Stokes equations for wave-vegetation interaction, and the formulas of drag coefficient and inertial coefficient were calibrated by using experimental data. Teh et al. (2009) introduced the Morison equation into a numerical model based on the Boussinesq equations and used the calibrated drag and inertial coefficient formulas in the simulation. Ma et al. (2013) developed a non-hydrostatic Reynolds

averaged Navier-Stokes equations (RANS) model to investigate the wave attenuation, turbulent mixing, and nearshore circulation induced by vegetation. A nonlinear k-ε model considering vegetation-induced turbulence production was used to study turbulent characteristics within the vegetation domain. Maza et al. (2015) used a three-dimensional numerical model based on IHFOAM to study the interaction of tsunami waves with mangrove forests.

In natural environments, waves and current can co-exist in coastal waters. However, due to the complex mechanics of wave-current-vegetation interaction, there are fewer studies on wave attenuation inside vegetation domain under current influences. Li and Yan (2007) conducted a flume experiment and numerical simulation to investigate wave-current-vegetation interaction and found that the presence of current will enhance wave attenuation. On the other hand, Paul et al. (2012) found that tidal current could reduce wave attenuation. Hu et al. (2014) found that the current could enhance or decrease wave attenuation, which was determined by the magnitude of the flow velocity ratio. Yin et al. (2020) investigated the effects of following and opposing currents on wave attenuation and found that the following currents could either enhance or suppress wave attenuation while the opposing currents always enhanced wave attenuation. Zhao et al. (2021) conducted a flume experiment and a numerical modeling based on the Boussinesq equations to study wave attenuation under the following and opposing currents conditions and found that the effect of current on wave attenuation depends on the magnitude of the velocity ratio. Chen et al. (2020) conducted a flume experiment to study the flow field structure and turbulence characteristics within and outside the submerged vegetation domain under wave-current conditions. So far, the effect of current on wave attenuation is yet to be clarified.

For theoretical studies, Hu et al. (2014) proposed a theoretical model (from herein it is referred to as Hu 2014 model) based on energy conservation and validated it by using experimental data. This model can predict the ratio of wave attenuation under wave-current conditions to that under pure wave condition. Since the Hu 2014 model does not consider the effect of wave-current interaction on changing wave group velocity, the predicted results under wave following current and wave opposing current are symmetric. Recently, Hu et al. (2022) conducted a flume experiment to study wave breaking induced by opposing current and extended Hu 2014 model for predicting wave attenuation induced by breaking waves and

opposing current in the submerged vegetation domain. Losada et al. (2016) extended the Dalrymple 1984 model for wave-current-vegetation interaction (from herein it is referred to as Losada 2016 model). This model can be used to investigate the bulk-averaged drag coefficient C_D under wave-current conditions. In the derivation of this model, the current velocity in the dense vegetation domain was considered to be small, and thus its contribution to the drag force could be ignored. These theoretical models assumes that wave decay still follows reciprocal law in wave-current-vegetation interaction, the same as that for wave-vegetation interaction (Dalrymple et al., 1984), even though such decay pattern could not be fully supported by the experimental data for strong currents (Hu et al., 2014).

In the present study, we develop a new theoretical model for wave decay inside an emerged vegetation domain under current influences by considering the current effects on changing both wave group velocity and energy dissipation rate. This model can be reduced to Dalrymple 1984 model when the current velocity is equal to zero. We will compare the present theoretical model with available experimental data and numerical simulations under different wave-current conditions. Special attentions will be paid to investigate current effect on the wave height decay characteristics under different current strength regimes, i.e., the ratio of current velocity to wave orbit velocity varies from 1.5 to 3.0.

2. Derivation of the theoretical model

2.1 Governing equation

In **Fig. 1,** considering a linear incident wave train of amplitude a_{w0} and period of T propagates over an emerged vegetation domain with a background uniform current, the wave amplitude will gradually decay due to the presence of the vegetation. The coordinate system is fixed on the still water level. We consider the domain of [0, L_v] where the vegetation is uniformly distributed along x-axes and let x=0 and x=L_v be where the emerged vegetation domain begins and ends, respectively. Denoting $a_w(x)$ as the wave amplitude as a function of x, we have $a_w(0)$ and $a_w(L_v)$ to be the wave amplitude at the beginning and the end of the emerged vegetation domain. The background current U_c is a constant in the entire domain. depending on the current direction, we have wave following current for U_c>0 and wave opposing current for

U_c<0. The vegetation is composed of rigid circular cylinders with density N (stem/m^2) and diameter D (m).

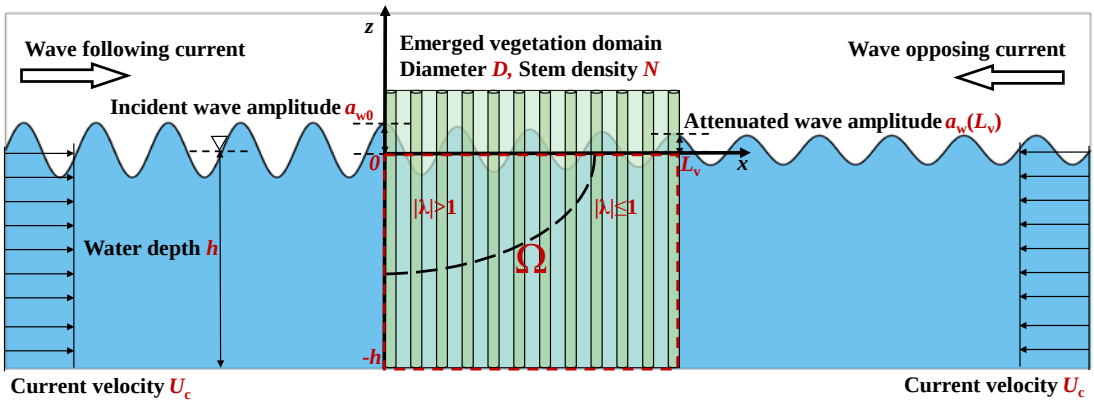

Fig. 1. A sketch of wave-current-vegetation interaction.

Denote $\Omega=[0, L_v]\times[-h, 0]$ to be the domain to be investigated. The conservation equation of wave energy flux under wave-current conditions can be written as:

$$\frac{\partial\left(E_{wc\_w}C_{g\_wc}\right)}{\partial x}=-\varepsilon_{wc\_w},\left(x,z\right)\in\Omega \tag{1}$$

where E_{wc_w} is the energy density of the wave under wave-current conditions, which is equal to

$$E_{wc\_w}=\frac{1}{2}\rho g a_w^{\ 2} \tag{2}$$

in which ρ is the fluid density (kg/m^3), g the gravitational acceleration (m/s^2), ε_{wc_w} the time-averaged rate of wave energy dissipation in the per unit length vegetation domain, and C_{g_wc} the group velocity of wave-current (m/s), which can be expressed as:

$$C_{g\_wc}=U_c+\frac{1}{2}\left(1+\frac{2kh}{\sinh 2kh}\right)\sqrt{\frac{g}{k}\tanh kh} \tag{3}$$

where k is the wavenumber obtained by solving the dispersion equation:

$$\left(\omega-U_c k\right)^2=gk\tanh kh \tag{4}$$

where $\omega=2\pi/T$ is the angular frequency of the wave.

According to Li and Yan (2007), the total energy dissipation ε_{wc} in the vegetation domain can be divided into two parts: the dissipation caused by the current ε_{wc_c} and the dissipation caused by the wave under the influence of wave-current interaction ε_{wc_w}. Therefore, the RHS of Eq. (1) can be written as:

$$-\varepsilon_{wc\_w} = -\left(\varepsilon_{wc} - \varepsilon_{wc\_c}\right) \tag{5}$$

Assuming the energy loss in the vegetation domain comes from the negative work done by the vegetation on the water flow, the energy dissipation terms in the RHS of Eq. (5) can be calculated by:

$$\varepsilon_{wc} = \frac{1}{T}\int_0^T dt \int_{-h}^0 uF_D dz \tag{6}$$

where F_D is the reaction force of the vegetation to the water flow and u is the wave orbit velocity. Based on the linear wave theory, the horizontal wave velocity can be written as:

$$u_w(t,z) = \frac{ga_w k}{\omega}\frac{\cosh k(z+h)}{\cosh kh}\sin(\omega t) \tag{7}$$

We assume that the instantaneous flow velocity is the linear superposition of the current velocity U_c and wave velocity u_w:

$$u(t,z) = U_c + u_w = U_c + \frac{ga_w k}{\omega}\frac{\cosh k(z+h)}{\cosh kh}\sin(\omega t) \tag{8}$$

According to the Morison equation, F_D can be expressed as:

$$F_D = \frac{1}{2}N\rho C_D D\left|U_c + \frac{ga_w k}{\omega}\frac{\cosh k(z+h)}{\cosh kh}\sin(\omega t)\right|\left\{U_c + \frac{ga_w k}{\omega}\frac{\cosh k(z+h)}{\cosh kh}\sin(\omega t)\right\} \tag{9}$$

and

$$\varepsilon_{wc\_c} = \frac{1}{2}Nh\rho C_D D|U_c|U_c{}^2 = \frac{1}{T}\int_0^T\int_{-h}^0 \frac{1}{2}N\rho C_D D|U_c|^3 dzdt \tag{10}$$

where C_D is the bulk-averaged drag coefficient.

Then we substitute Eqs. (6), (8), (9), and (10) into Eq. (5) and have:

$$\begin{aligned}&-\frac{\partial\frac{1}{2}\rho g a_w{}^2 C_{g\_wc}}{\partial x}\\ &=\frac{1}{T}\int_0^T\int_{-h}^0\frac{1}{2}N\rho C_D D\left|U_c + \frac{ga_w k}{\omega}\frac{\cosh k(z+h)}{\cosh kh}\sin(\omega t)\right|\left[U_c + \frac{ga_w k}{\omega}\frac{\cosh k(z+h)}{\cosh kh}\sin(\omega t)\right]^2 dzdt\\ &-\frac{1}{T}\int_0^T\int_{-h}^0\frac{1}{2}N\rho C_D D|U_c|^3 dzdt\end{aligned} \tag{11}$$

Making transformation of the integral variable t with $\tau=\omega t$, after simplification, Eq. (11) can be expressed as:

$$-\frac{\partial\left(\frac{1}{2}\rho g a_w{}^2 C_{g\_wc}\right)}{\partial x} = \frac{N\rho C_D D}{4\pi}\int_0^{2\pi}|U_c|^3 dz\int_{-h}^0\left[\left|1 + \frac{ga_w k}{U_c\omega}\frac{\cosh k(z+h)}{\cosh kh}\sin\tau\right|^3 - 1\right]d\tau$$

(12)

Eq. (12) is a boundary value problem (BVP), describing the variation of the wave amplitude inside the vegetation domain.

2.2 Theoretical solution

It's worth indicating that the most difficult part of solving Eq. (12) lies in deriving the explicit solution of the double integral on the right side of the equation. Due to the presence of absolute values in the integrand function, the expression of the integral result is not unique, which depends on the value of the coefficient in front of sin(τ). Therefore, in the derivation, we need to discuss the value of this coefficient first. For simplicity in derivation, we re-write the double integral to:

$$I_1 = \int_{-h}^{0} \left|U_c\right|^3 \mathrm{d}z \int_0^{2\pi} \left[\left|1+\lambda\left(x,z\right)\sin\left(\tau\right)\right|^3 - 1 \right] \mathrm{d}\tau \tag{13}$$

where

$$\lambda\left(x,z\right) = \frac{g a_w k}{U_c \omega} \frac{\cosh k\left(z+h\right)}{\cosh kh} \tag{14}$$

Introducing the following constant ratio of the maximum wave orbital velocity to the uniform current velocity:

$$\alpha_r = \frac{U_c}{g a_{w0} k / \omega} \tag{15}$$

where a_{w0} is the wave amplitude at x=0, Eq. (14) can be re-written as:

$$\lambda\left(x,z\right) = \frac{1}{\alpha_r} \frac{a_w \cosh k\left(z+h\right)}{a_{w0} \cosh kh} \tag{16}$$

Since the wave amplitude attenuates gradually as it moves through the vegetation domain, leading to the maximum and minimum of $a_w(x)$ as $a_w(0)$ and $a_w(L_v)$. In addition, at the same x position, the wave has the maximum orbital velocity at $z=0$ and minimum velocity at $z=-h$. Thus, according to Eq. (16) and (15), for each $(x,z)\in\Omega$, the inequality for $\lambda(x,z)$ yields:

$$\frac{\gamma}{\left|\alpha_r\right|} \le \left|\lambda(x,z)\right| \le \frac{1}{\left|\alpha_r\right|} \tag{17}$$

and

$$\gamma = \frac{a_{\mathrm{w}}\left(L_{\mathrm{v}}\right)}{a_{\mathrm{w0}}}\frac{1}{\cosh kh} \tag{18}$$

which γ is a constant.

To solve the second integral of Eq. (13), we denote the time integral term as the following equation:

$$M\left(\lambda\right) = \int_0^{2\pi}\left[\left|1+\lambda\sin\left(\tau\right)\right|^3 - 1\right]\mathrm{d}\tau \tag{19}$$

where λ is abbreviated to $\lambda(x,z)$ and $M(\lambda)$ is a parametric integral with respect to λ. Thus, the governing equation (12) and I_1 can be rewritten as follows in terms of $M(\lambda)$:

$$-\frac{\partial\left(\frac{1}{2}\rho g {a_{\mathrm{w}}}^2 C_{\mathrm{g\_wc}}\right)}{\partial x} = \frac{N\rho C_{\mathrm{D}} D}{4\pi} I_1 \tag{20}$$

and

$$I_1 = \int_0^{2\pi}\left|U_{\mathrm{c}}\right|^3 d\tau M\left(\lambda\right) \tag{21}$$

We find that the integral results of Eq. (19) will be completely different for $|\lambda|\leq 1$ and $|\lambda|>1$, which requires different solution techniques. In addition, the domain of values of λ is determined by the constant α_{r} according to Eq. (17). Thus, we need to find solutions of the differential equation Eq. (12) in terms of different value of α_{r}. In the following sections, we will derive the solutions of $a_{\mathrm{w}}(x)$ when $|\alpha_{\mathrm{r}}|\geq 1$, $1-\delta\leq|\alpha_{\mathrm{r}}|\leq 1$, $|\alpha_{\mathrm{r}}|\leq\delta$, and $\delta\leq|\alpha_{\mathrm{r}}|\leq 1-\delta$, where $0<\delta\ll 1$.

2.2.1 Exact solution for $|\alpha_{\mathrm{r}}|\geq 1$ (strong current)

We first obtain an exact solution for $a_{\mathrm{w}}(x)$, $(0\leq x\leq L_{\mathrm{v}})$, where the absolute value of the current velocity is always greater than or equal to that of wave velocity ($|\alpha_{\mathrm{r}}|\geq 1$). Based on Eq. (17), the following relation can be obtained:

$$\left|\lambda\left(x,z\right)\right| \leq \frac{1}{\left|\alpha_{\mathrm{r}}\right|} \leq 1 \tag{22}$$

Thus, back to Eq. (19), the absolute value sign of the integrand function in $M(\lambda)$ can be removed for every $(x,z)\in\Omega$, leading to the explicit result:

$$M\left(\lambda\right) = \int_0^{2\pi}\left[\left(1+\lambda\sin\tau\right)^3 - 1\right]\mathrm{d}\tau = \int_0^{2\pi}\left(\lambda^3\sin^3\tau + 3\lambda^2\sin^2\tau + 3\lambda\sin\tau\right)\mathrm{d}\tau = 3\pi\lambda^2 \tag{23}$$

Since the explicit result is obtained and note that λ satisfies Eq. (16), then the integral I_1 can be

calculated according to Eq. (21):

$$I_1 = \frac{3\pi a_w{}^2 g^2 k |U_c| \left(\tanh kh + kh \operatorname{sech}^2 kh\right)}{2\omega^2} \tag{24}$$

Thus, the governing equation Eq. (20) can be simplified with the use of Eq. (24):

$$-\frac{1}{2}\rho g C_{g\_wc} \frac{\partial a_w{}^2}{\partial x} = \frac{C_D D N \rho}{4\pi} \left[\frac{3\pi a_w{}^2 g^2 k |U_c| \left(\tanh kh + kh \operatorname{sech}^2 kh\right)}{2\omega^2} \right] \tag{25}$$

Eq. (25) is an ordinary differential equation for $a_w(x)$, ($0 \le x \le L_v$). By solving the governing equation and boundary condition, the exact solution of the wave amplitude in the emerged vegetation domain is derived:

$$a_w(x) = a_{w0} \exp(-mx) \tag{26}$$

where m is a constant independent of x:

$$m = \frac{3 C_D D g k N |U_c| \operatorname{sech}^2 kh \left(2kh + \sinh 2kh\right)}{16 C_{g\_wc} \omega^2} \tag{27}$$

2.2.2 Asymptotic solution for $(1-\delta) \le |\alpha_r| \le 1$ (intermediately strong current)

When $1-\delta \le |\alpha_r| \le 1$, the exact solution does not exist. However, an asymptotic solution exists for $a_w(x)$ given $\delta << 1$. Based on Eq. (17), we have:

$$|\lambda(x,z)| \le \frac{1}{|\alpha_r|} \le \frac{1}{1-\delta} \tag{28}$$

Because the right-hand term of Eq. (28) is greater than 1, $|\lambda(x,z)| \le 1$ will be true only for part of $(x,z) \in \Omega$. Thus, different from the derivation in section 2.2.1, we have to consider the result of $M(\lambda)$ for $|\lambda| > 1$. Considering that the solution for Eq. (19) is a piecewise function, as shown in **Fig. 1**, the vegetation domain can be divided into two parts corresponding to $|\lambda| > 1$ and $|\lambda| \le 1$, and we have:

$$M(\lambda) = \begin{cases} 3\pi\lambda^2 & |\lambda| \le 1 \\ 3\sqrt{\lambda^2 - 1}\left(\lambda^2 + 4\right) - 2i\left(3\lambda^2 + 2\right) S_1 + 3i\lambda^2 \sinh 2S_1 - \frac{1}{3}\lambda^3 \cosh 3S_1 - 2\pi & |\lambda| > 1 \end{cases} \tag{29}$$

and

$$S_1 = \log\left(\frac{\sqrt{\lambda^2 - 1} + i}{\lambda}\right) \tag{30}$$

where i is the unit imaginary. The expression of $M(\lambda)$ ($|\lambda|>1$) is so complex that it is difficult to obtain the explicit result for I_1 when $M(\lambda)$ is applied as the integrand function in Eq. (13). To simplify the expression for $M(\lambda)$ for $|\lambda|>1$, we make a polynomial approximation by applying a second order Taylor expansion to $M(\lambda)$ at $|\lambda|=1$, and then the following expression is obtained:

$$M(\lambda) = 3\pi\lambda^2 + o\left(\delta^2\right),\ |\lambda| > 1 \tag{31}$$

where $o(\delta^2)$ is a second-order infinitesimal about δ. With the expansion Eq. (31), the expression of $M(\lambda)$, Eq. (29), can be further rewritten as:

$$M(\lambda) = 3\pi\lambda^2 + o\left(\delta^2\right),\ |\lambda| \le \frac{\delta}{1-\delta} \tag{32}$$

which means that for each $(x,z)\in\Omega$, $M(\lambda)$ can always be expressed as Eq. (32). Then the integral I_1 can be obtained according to Eq.(24):

$$I_1 = \frac{3\pi a_w{}^2 g^2 k |U_c| \left(\tanh kh + kh\,\mathrm{sech}^2 kh\right)}{2\omega^2} + o\left(\delta^2\right) \tag{33}$$

It is noted that if we ignore high order infinitesimal $o(\delta^2)$, the approximate result for I_1 is the same as Eq. (24), leading to the final asymptotic solution sharing the same solution form of $a_w(x)$ as in Eq. (26) and (27).

2.2.3 Asymptotic solution for $|\alpha_r|\le\delta$ (weak current)

In this section, we derive an asymptotic solution for $a_w(x)$ when $|\alpha_r|\le\delta$. Firstly, from Eq. (17), the domain of values of $\lambda(x,z)$ can be estimated:

$$\frac{\gamma}{\delta} \le \frac{\gamma}{|\alpha_r|} \le |\lambda(x,z)| \tag{34}$$

when the small parameter $\delta\to 0$, the term on the left-hand side of the inequality in Eq. (34) will tend to positive infinity, leading to $|\lambda(x,z)|\to+\infty$. Thus, the Taylor expansion, Eq. (31) for $M(\lambda)$ at $|\lambda|=1$ will fail, which motivates us to find another polynomial approximation for $M(\lambda)$. Since $\lambda(x,z)$ is independent of the integral in Eq. (19), through identical deformation, $M(\lambda)$ can be rewritten as:

$$M(\lambda)=|\lambda|^3\tilde{M}(\mu) \tag{35}$$

and

$$\tilde{M}(\mu)=\int_0^{2\pi}\left[\left|\mu+\sin(\tau)\right|^3-\mu^3\right]\mathrm{d}\tau \tag{36}$$

where $\mu=\mu(x,z)$ is a newly introduced function, satisfying:

$$\mu=\lambda^{-1} \tag{37}$$

Further, the inequality Eq. (34) can be expressed as the following form, in terms of μ:

$$|\mu|\le\delta\gamma^{-1}\ll 1 \tag{38}$$

When $|\mu|<1$, the expression for Eq. (36) can be obtained:

$$\tilde{M}(\mu)=3\pi\mu+\frac{2}{3}\sqrt{1-\mu^2}\left(4+11\mu^2\right)-\mu\left(3+4\mu^2\right)\arccos\mu+3i\mu\log\left(\mu+i\sqrt{1-\mu^2}\right) \tag{39}$$

which is the exact solution for $\tilde{M}(\mu)$ ($|\mu|<1$). However, it's too complex as an integrand function. Then, we can expand $\tilde{M}(\mu)$ at $\mu=0$ up to the second order in Taylor series form, for each $(x,z)\in\Omega$:

$$\tilde{M}(\mu)=\frac{8}{3}+12\mu^2+o\left[\left(\delta\gamma^{-1}\right)^2\right] \tag{40}$$

Then the integral I_1 can be obtained according to Eq. (13), (21), (35), (37):

$$I_1=\frac{4\tanh kh\left(4{a_w}^3g^3k^2\operatorname{sech}^2kh+2{a_w}^3g^3k^2+27a_wg{U_c}^2\omega^2\right)}{9\omega^3}+o[(\delta\gamma^{-1})^2] \tag{41}$$

For further simply, we introduce a function $\xi=\xi(x)$ which depends only on x:

$$\xi(x)=\frac{U_c\omega}{ga_w(x)k} \tag{42}$$

Based on Eq. (42), the current velocity U_c can be expressed as:

$$U_c=\frac{\xi(x)ga_w(x)k}{\omega} \tag{43}$$

when $x=0$,

$$\xi(0)=\frac{U_c\omega}{ga_w(0)k} \tag{44}$$

where $\xi(0)$ is equal to α_r, and we assume that $\xi(x)$ varies slowly with x, which leads to:

$$\xi(x)=\xi(0)+o(\xi(0)) \tag{45}$$

If we ignore infinitesimal $o(\alpha_r)$ in Eq. (45), then Eq. (43) can be rewritten as:

$$U_c\approx\frac{\xi(0)ga_w(x)k}{\omega} \tag{46}$$

If we replace U_c in Eq. (41) with Eq. (46), the governing equation Eq. (20) is obtained:

$$-\frac{1}{2}\rho g C_{g\_wc}\frac{\partial a_w^{\ 2}}{\partial x}=\frac{C_D D N\rho}{4\pi}\left[\frac{4a_w^{\ 3}g^3k^2\tanh kh(27\xi(0)^2+4\mathrm{sech}^2 kh+2)}{9\omega^3}\right] \quad (47)$$

After solving the ordinary differential equation Eq. (47), the approximate solution for $a_w(x)$ is derived:

$$a_w(x)=\frac{a_{w0}}{1+m'x} \quad (48)$$

and m' is a constant independent to x.

$$m'=\frac{a_{w0}NC_D Dg^2k^2\left[2+27(\frac{U_c}{ga_{w0}k/\omega})^2+4\mathrm{sech}^2 kh\right]\tanh kh}{9\pi C_{g\_wc}\omega^3} \quad (49)$$

If we introduce the dispersion equation and the expression of group velocity into Eq. (49) and simplify this equation, we can get a new expression of m':

$$m'=\frac{8a_{w0}NC_D Dk\left[\frac{27U_c^{\ 2}\sinh^2 kh\cosh kh}{2a^2_{\ w0}gk}+\sinh^3 kh+3\sinh kh\right]}{9\pi\left(\frac{4U_c\omega\cosh^2 kh}{g}+2kh+\sinh 2kh\right)\sinh kh} \quad (50)$$

When U_c=0, Eq. (50) can be reduced to the theoretical formula derived by Dalrymple et al. (1984) for predicting the wave attenuation in a uniform distributed rigid cylindrical group in the absence of background current which m' is expressed as:

$$m'=\frac{8a_{w0}NC_D Dk\left(\sinh^3 kh+3\sinh kh\right)}{9\pi(\sinh 2kh+2kh)\sinh kh} \quad (51)$$

2.2.4 Approximate solution for $\delta\leqslant|\alpha_r|\leqslant 1-\delta$ (intermediate current)

For $\delta\leq|\alpha_r|\leq 1-\delta$, it is difficult to find a theoretical solution. By observing that the decay rate changes smoothly with current velocity in this range, we propose to construct a linear combination solution from the known solutions derived previously at $|\alpha_r|=\delta$ and $|\alpha_r|=1-\delta$:

$$a_w(x)=\alpha_1 a_{w0}\exp(-mx)+(1-\alpha_1)\frac{a_{w0}}{1+m'x},\left(\delta<|\alpha_r|<1-\delta\right) \quad (52)$$

and the weight coefficient is calculated by:

$$\alpha_1=-\frac{1}{1-2\delta}\left(|\alpha_r|+\delta-1\right),\left(\delta<|\alpha_r|<1-\delta\right) \quad (53)$$

where the expression of m and m' can be referred to Eq. (27) and (49), respectively.

2.3 Determination of δ and Error analysis

We now need to complete the solution procedure by determining the proper value of δ. For the convenience of application, we divide the interval of $|\alpha_r|$ from 0 to 1 into three equal segments with the length of 1/3, and the final expression can be rewritten as:

$$a_w(x)/a_{w0}=\begin{cases}\dfrac{1}{1+\dfrac{a_{w0}NC_D Dg^2k^2\left[2+27(\dfrac{U_c}{ga_{w0}k/\omega})^2+4\mathrm{sech}^2 kh\right]\tanh kh}{9\pi C_{g\_wc}\omega^3}x} & |\alpha_r|\le\dfrac{1}{3}\\ (-3|\alpha_r|+2)\dfrac{1}{1+\dfrac{a_{w0}NC_D Dg^2k^2\left[2+27(\dfrac{U_c}{ga_{w0}k/\omega})^2+4\mathrm{sech}^2 kh\right]\tanh kh}{9\pi C_{g\_wc}\omega^3}x} & \\ +(3|\alpha_r|-1)\exp\left[-\dfrac{3C_D DgkN|U_c|\mathrm{sech}^2 kh(2kh+\sinh 2kh)}{16C_{g\_wc}\omega^2}x\right] & \dfrac{1}{3}<|\alpha_r|<\dfrac{2}{3}\\ \exp\left[-\dfrac{3C_D DgkN|U_c|\mathrm{sech}^2 kh(2kh+\sinh 2kh)}{16C_{g\_wc}\omega^2}x\right] & |\alpha_r|\ge\dfrac{2}{3}\end{cases} \quad (54)$$

Since the above expression contains both asymptotic solution and approximate solution for $|\alpha_r|<1$, it is important to understand the relative errors introduced during the approximation. To achieve this objective, the calculation results based on Eq. (54) are compared to the finite difference results solving the original ordinary differential Eq. (11) directly:

$$\frac{a_{w,n}^{\ 2}-a_{w,n-1}^{\ 2}}{\Delta x}=-\frac{\varepsilon_{wc}-\varepsilon_{wc\_c}}{\frac{1}{2}\rho g C_{g\_wc}} \quad (55)$$

in which Δx is the grid size in the x-direction, $a_{w,n}$ is the wave amplitude at $x=n\Delta x$, and n is range from 1 to $L_v/\Delta x$. Starting from the incident wave amplitude $a_{w,0}$ at the edge of the vegetation domain (x=0), the wave amplitude at each location ($a_{w,n}$) is calculated by the wave amplitude at the previous position ($a_{w,n-1}$). When Δx approaches 0, the finite difference solution can be regarded as the true solution of Eq. (11). The above finite difference solution is solved by Wolfram Mathematica.

The comparison is made for the case of water depth h=0.8 m, incident wave amplitude a_{w0}=0.05 m, wave period T=1.8 s, vegetation diameter D=0.008 m, vegetation density N=333

stem/m^2, and current velocity U_c ranging from -0.4 m/s to 0.8 m/s. C_D is selected as 1.31. The domain of interest has the length of 4.2 m, the same as the wavelength without current, and it is divided into 600 meshes with Δx=0.007m.

The abscissa of **Fig. 2** is the ratio of current velocity U_c to pure wave orbital velocity u_{w0}, the left ordinate is the comparison of wave attenuation rate K_v:

$$K_v = 1 - a_w(L_v) / a_w(0) \tag{56}$$

and the right ordinate is the relative error ψ:

$$\psi = \frac{\left| K_{vD} - K_{vP} \right|}{K_{vD}} \tag{57}$$

where K_{vD} is from the finite-difference solution and K_{vP} is from the present model.

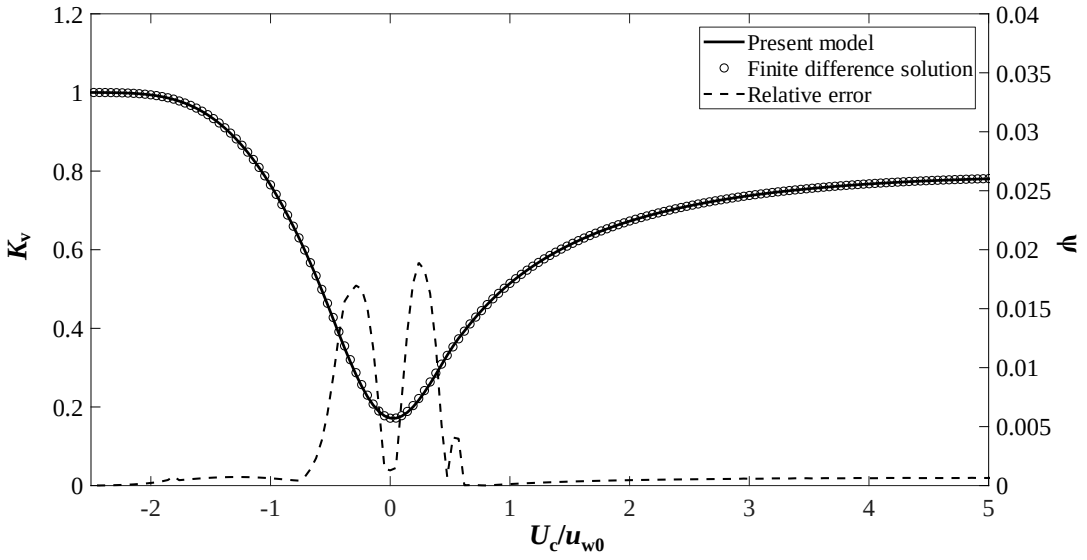

Fig. 2. Comparison of the present model with the finite difference solution and the relative error analysis.

From **Fig. 2** we can find that the theoretical model is in generally good agreement with the finite-difference solution. The relative error reaches the maximum of 2.4% when U_c/u_{w0} equals 0.19. When the absolute value of α_r is greater than 1, the theoretical model is based on exact solution, and the relative error here mainly comes from the truncation errors from the finite-difference scheme, which is less than 0.1%.

3. Discussions of the present theoretical model

Inspecting Eq. (54) and referring to Fig. 2, we are able to find the following characteristics of wave damping inside the vegetation domain under current influence:

1. Due to the change of current direction, the group velocity of wave opposing current is smaller than that of wave following current under the same current speed. Consequently, when the drag force coefficient C_D is constant, the wave height attenuation for wave opposing current will be larger than that for wave following current, which is also clearly shown in **Fig. 2**.
2. As the absolute value of velocity ratio increases, the decaying law of wave height will change from reciprocal decay to exponential decay. For a weak current velocity U_c, the LHS of Eq. (47) is correlated with $a_w(x)^2$ and the RHS of Eq. (47) is correlated with $a_w(x)^3$, the decaying law is thus of reciprocal form. For a strong current velocity U_c, both the LHS and RHS of Eq. (25) are related to $a_w(x)^2$, and Eq. (25) can be reduced to a linear equation that dictates an exponential decay.
3. When the current is weak, a larger incident wave height will induce larger wave height decay, whereas the decay rate is independent of incident wave height when the current is strong (i.e., the absolute value of velocity ratio is greater than 2/3). This is because when the current is strong, the LHS and RHS of Eq. (25) are both related to $a_w(x)^2$, thus, the decay rate is no longer related to the incident wave amplitude a_{w0}.

In the following paragraphs, we will discuss these wave decaying properties in detail, together with available experimental data and numerical results.

3.1 Effect of the current directions on wave height attenuation

The present model indicates that the wave height attenuation shows an asymmetric dependency on the current direction. To demonstrate this phenomenon, the present model will be compared with the experimental data of Zhao et al. (2021). The main experimental setup is shown in **Table 1**.

Table 1 Experimental setup of Zhao et al. (2021)

D (m)	N (stem/m^2)	h_v (m)	L_v (m)	Period (s)	U_c (m/s)
0.005	555	0.6	5	1.5, 2.0	-0.19, -0.1, 0.1, 0.2

Although the incident wave amplitudes range from 0.02 m to 0.04 m, the actual wave amplitudes at the front face of the vegetation domain range roughly from 0.015 m to 0.045 m due to wave-current interactions. Therefore, in the theoretical model, we adopt the range of a_{w0}=0.015 m – 0.045 m. The drag coefficient C_D is selected as 1.31.

Fig. 3 shows the comparisons of wave attenuation rates between the experimental data and calculations from the present theoretical models. Both experimental data and theoretical results have a clear trend that the wave decaying rate is larger in the opposing current conditions. The envelop calculated by the theory well predicts the behavior of wave decaying observed in the laboratory. Another interesting finding is that for the same current speed, the decaying rate is normally positively correlate to the wave amplitude, i.e., the decaying rate increases as the increase of wave amplitude. Both the theory and the experimental data confirm this decaying property.

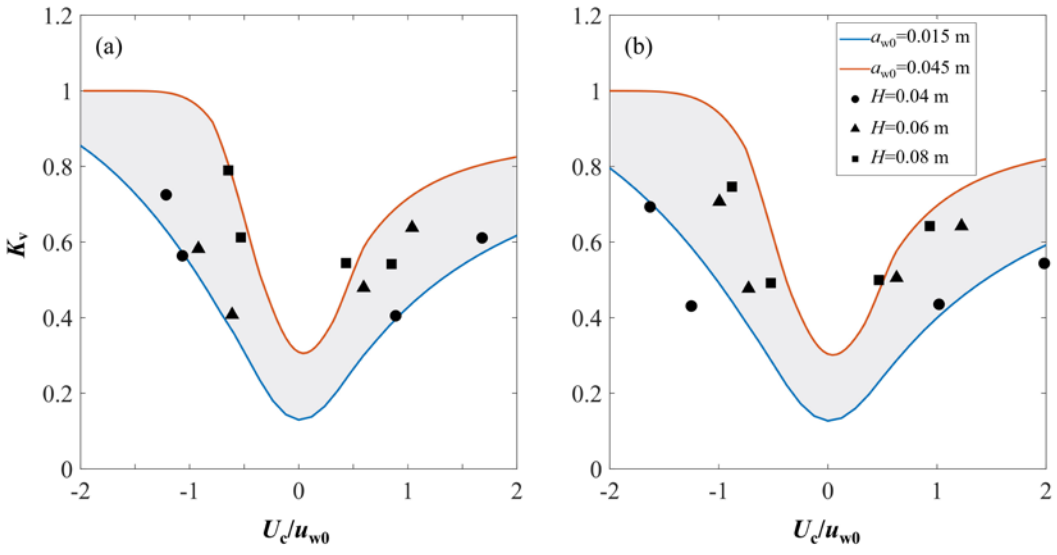

Fig. 3. Comparison of wave attenuation rate between the experimental data (symbols) of Zhao et al. (2021) and the present model (lines) for (a) wave period T=1.5 s and (b) wave period T=2.0 s.

3.2 Variation of decaying laws with respect to current speed

In the present model, the wave attenuation follows reciprocal decay for weak current but

exponential decay for strong current. For intermediate current strength, i.e., $1/3<|\alpha_r|<2/3$, it is a mixture of exponential and reciprocal decay. To better understand how current speed affects the decaying law of wave height in vegetation domain, we decide to compare the present model with available experimental data and numerical results from a RANS model to further explore the different decaying laws in different flow regimes.

The 2-D RANS model NEWFLUME was first proposed by (Lin and Xu, 2006; Lin, 2008) and extended by Tang et al. (2021) for simulation of wave and current interaction with vegetation. In the numerical model, the vegetation is idealized by a group of rigid circular cylinders and treated as a domain of porous media. The double-averaged method based on the original Navier-Stokes equations is employed. The resulting governing equations are:

$$\frac{\partial \langle \overline{u}_i \rangle}{\partial x_i} = 0 \tag{58}$$

$$\frac{1}{\theta}\frac{\partial}{\partial t}\langle \overline{u}_i \rangle + \frac{\langle \overline{u}_j \rangle}{\theta^2}\frac{\partial}{\partial x_j}\langle \overline{u}_i \rangle = -\frac{1}{\rho}\frac{\partial}{\partial x_i}\langle \overline{p} \rangle + \frac{\nu}{\theta}\frac{\partial^2}{\partial x_j \partial x_j}\langle \overline{u}_i \rangle + g_i - \frac{1}{\theta^2}\frac{\partial}{\partial x_j}\left\langle \overline{u_i' u_j'} \right\rangle - \left\langle \overline{f_i} \right\rangle \tag{59}$$

where the bracket represents the volume averaging and the overbar denotes the ensemble averaging. $\langle \overline{u}_i \rangle$ is the double-averaged velocity and i=1, 2, 3 for a three-dimensional flow, $\langle \overline{p} \rangle$ is the double-averaged pressure field, $\left\langle \overline{u_i' u_j'} \right\rangle$ is the double-averaged Reynolds shear stress which needs to be close by a turbulence closure model. θ is the porosity of the vegetation domain, and v is the dynamic molecular viscosity of fluid.

The force term $\left\langle \overline{f_i} \right\rangle$ in the Eq. (59) represents the horizontal reaction force from vegetation which includes drag force and inertial force. Since we ignore the effects of inertial force and the vertical drag force in present model, in order to be consistent with the model, we also omit the inertial force term and vertical drag force term in the numerical simulation, and the horizontal drag force can be calculated by Morison equation as:

$$\left\langle \overline{f_i} \right\rangle = \frac{2(1-\theta)}{\pi D}\rho C_D \left| \langle \overline{u} \rangle \right| \langle \overline{u} \rangle \tag{60}$$

A modified k-ε model consisting of shear-production term and wake-production term is used to close the Reynolds shear stress term and is expressed as:

$$\frac{\partial\langle\bar{k}\rangle}{\partial t}+\left\langle\bar{u}_j\right\rangle\frac{\partial\langle\bar{k}\rangle}{\partial x_j}=\frac{\partial}{\partial x_j}\left[\left(\nu+\frac{\nu_t}{\sigma_k}\right)\frac{\partial\langle\bar{k}\rangle}{\partial x_j}\right]+P_s+P_w-\langle\bar{\varepsilon}\rangle \tag{61}$$

$$\frac{\partial\langle\bar{\varepsilon}\rangle}{\partial t}+\left\langle\bar{u}_j\right\rangle\frac{\partial\langle\bar{\varepsilon}\rangle}{\partial x_j}=\frac{\partial}{\partial x_j}\left[\left(\nu+\frac{\nu_t}{\sigma_\varepsilon}\right)\frac{\partial\langle\bar{\varepsilon}\rangle}{\partial x_j}\right]+D_s+D_w-C_{\varepsilon 2}\frac{\langle\bar{\varepsilon}\rangle^2}{\langle\bar{k}\rangle} \tag{62}$$

in which ν_t is the eddy viscosity, σ_k, σ_ε, $C_{\varepsilon 1}$, and $C_{\varepsilon 2}$ are the empirical coefficients which are the same as the standard k-ε turbulence model, and the values are 1.0, 1.3, 1.44, and 1.92. P_s is the shear turbulence production term:

$$P_s=-\left\langle\overline{u_i'u_j'}\right\rangle\frac{\partial\left\langle\bar{u}_i\right\rangle}{\partial x_j} \tag{63}$$

P_w is the wake turbulence production term:

$$P_w=F_2\left(\frac{P_s}{P_w}\right)\eta_k\left\langle\bar{u}_i\right\rangle\left\langle\bar{f}_i\right\rangle \tag{64}$$

The formula $F_2()$ is a damping function which is introduced to suppress the vegetation wake production term inside the vegetation domain if the shear turbulence production term is dominant:

$$F_2\left(\frac{P_s}{P_w}\right)=\min\left[\exp\left(-\frac{P_s}{P_w}\right),1\right] \tag{65}$$

D_w represents the turbulence dissipation by vegetation:

$$D_w=\frac{C_{\varepsilon 2}}{\gamma}F_2\left(\frac{P_s}{P_w}\right)P_w^{\frac{4}{3}}d^{-\frac{2}{3}} \tag{66}$$

We select the experimental data of Hu et al. (2014) to compare with the present model and numerical simulation. The water depth h is 0.25 m, and the height of vegetation is 0.33 m. The vegetation domain length is 6 m, the vegetation density N is 556 stem/m^2, and the vegetation diameter is 0.01 m. The velocity ratio α_r and drag coefficient C_D are shown in **Table 2**, and the case name is defined by the combination of incident wave height, wave period, and current velocity, for example, Wave 0410 represents the incident wave height is 0.04 m and the wave period is 1.0 s.

Table 2 The values of velocity ratio α_r and drag coefficient C_D

Cases	α_r	C_D

Wave1015, U_c=0 m/s	0	1.5
Wave1015, U_c =0.05 m/s	0.15	1.3
Wave1015, U_c =0.15 m/s	0.49	0.95
Wave0410, U_c =0.2 m/s	1.59	0.75

The comparison of the relative wave amplitude variation in the vegetation domain is shown in **Fig. 4**. From **Fig. 4 (a)** to **Fig. 4 (d)**, the velocity ratio α_r changes from 0 to 1.59. The black triangles represent the numerical results, the black circles represent the experimental data, the red lines are the results predicted by the present model, the upper dotted lines represent the exponential decay, and the lower dotted lines represent reciprocal decay, respectively.

Fig. 4 (a) shows the comparison of the relative wave amplitude variation in the vegetation domain under pure wave conditions. The experimental data, present model, and numerical simulation all follow the reciprocal decay. When the current velocity is equal to 0.05 m/s which means weak current, **Fig. 4 (b)** shows that the present model and numerical simulation both conform to the reciprocal decay just as the experimental data. As the current velocity increase to intermediate flow, as shown in **Fig. 4 (c)**, the present model exhibits a mixture of reciprocal decay and exponential decay which is similar to the experimental data and numerical simulation. As shown in **Fig. 4 (d)**, when the current velocity increases to the strong current, the experimental data, numerical simulation, and the present model all follow the exponential decay.

In summary, the decaying laws of wave height attenuation within the vegetation domain are related to the velocity ratio α_r. When the absolute value of velocity ratio α_r is zero or close to zero, it appears as a reciprocal decay, when the value is greater than one, it appears as an exponential decay, and in the intermediate interval it is a mixture of reciprocal and exponential decay.

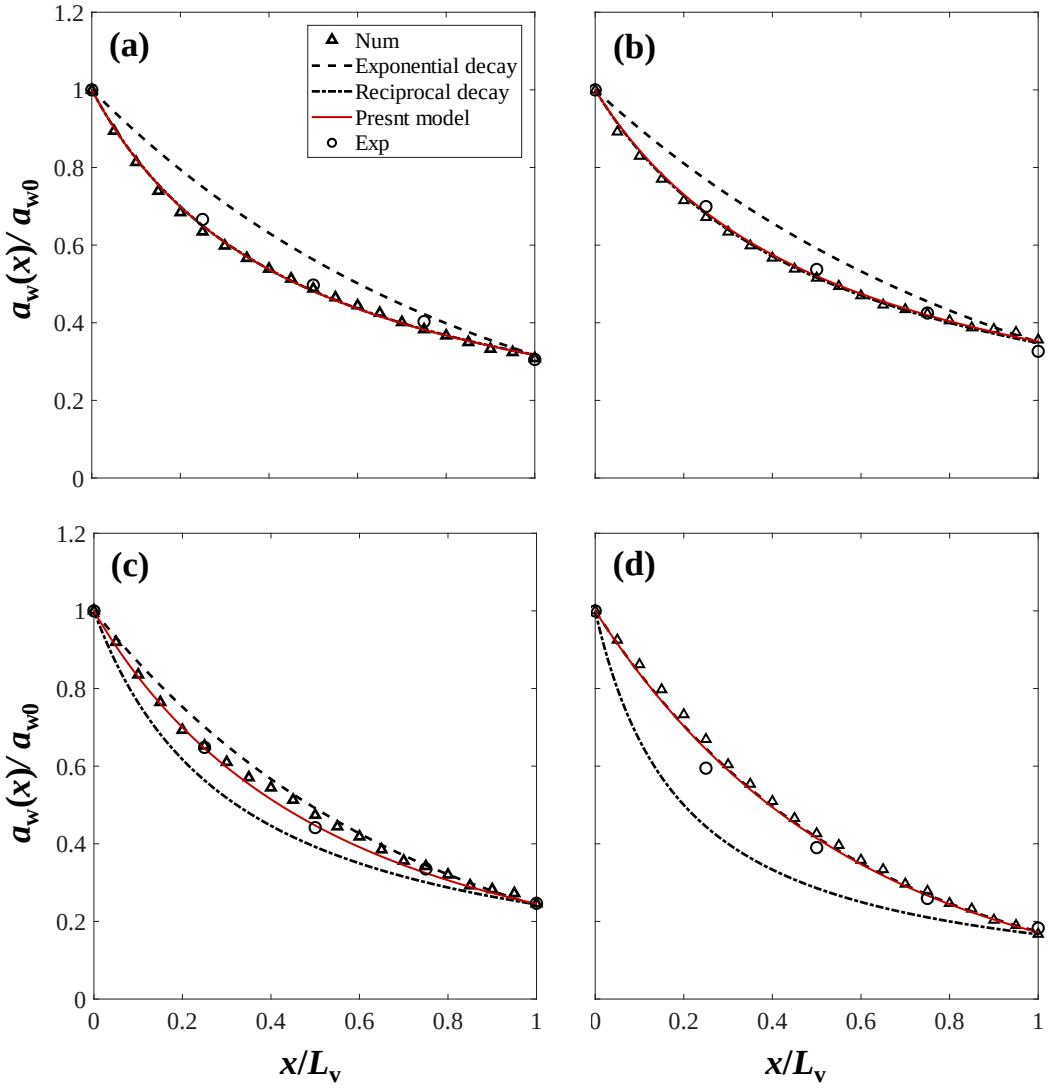

Fig. 4. Comparison of the relative wave amplitude variation of experimental data with numerical simulation and present model in terms of (a) Wave 1015, U_c =0 m/s, α_r=0, (b) Wave 1015, U_c =0.05 m/s, α_r=0.15, (c) Wave 1015, U_c =0.15 m/s, α_r=0.49, (d) Wave 0410, U_c =0.2 m/s, α_r=1.59.

Moreover, the turbulence intensity distribution and flow fields of case Wave1015U_c0.15 are shown in **Fig. 5**. The black box represents the vegetation domain, and the front position of the vegetation domain is defined as x=0 m. The moment when the wave crest reaches x=0 m is t=0. It can be observed that the flow field and turbulence intensity distribution are influenced by both wave and current. The maximum values of flow velocity and turbulence intensity occur at the moment when the wave crest is reached and the minimum values occur at the moment when the wave trough occurs. At the wave crest, the maximum values of flow velocity and

turbulence intensity appear at the free surface and gradually decrease with the increase of water depth. The waves gradually decay in the vegetation domain, and as the wave decay, the amplitude of the flow velocity decreases accordingly, leading to a decrease in turbulence intensity.

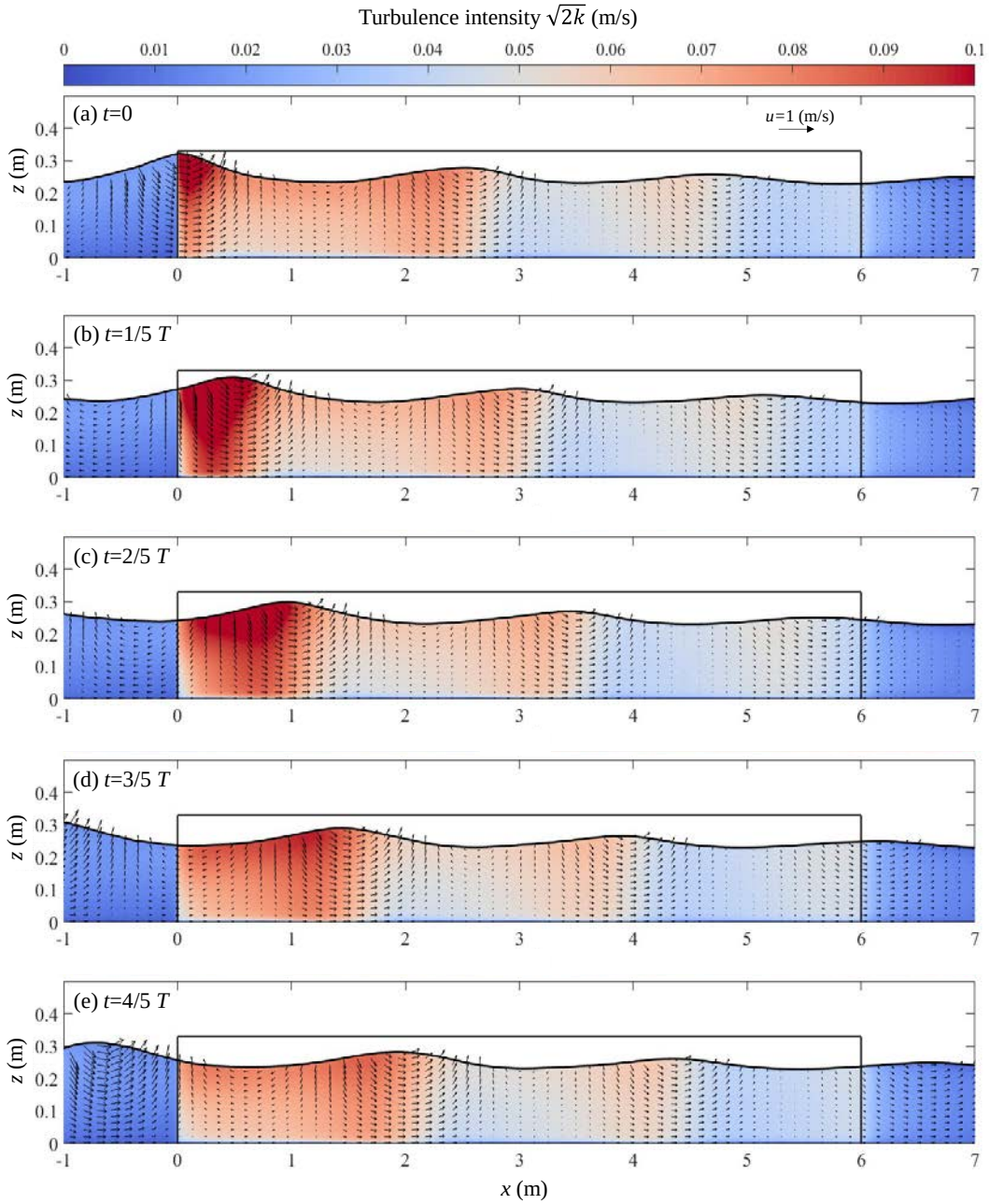

Fig. 5. The variation of flow field and turbulence intensity distribution in a wave period.

3.3 Wave height effect on the wave attenuation rate

According to the present model which is expressed in Eq. (54), we can find that if the drag coefficient C_D is a constant value, when the velocity ratio α_r is less than two-thirds, the wave attenuation rate is related to the incident wave amplitude and current velocity. However, when the velocity ratio α_r is greater than two-thirds, the wave attenuation rate is only related to the current velocity and independent of the incident wave amplitude.

To demonstrate this finding, the present model will be compared with the experimental data of Hu et al. (2014). In this comparison, the experimental data of vegetation density N =139 stem/m^2 is selected. The information about the wave-current and drag coefficient is listed in **Table 3**. The case name definition is the same as **Table 2**. There are two current velocities in the comparison. When U_c is equal to 0.05 m/s, the velocity ratio α_r is less than 2/3 for all cases, while when U_c is equal to 0.2 m/s, α_r is greater than 2/3.

Table 3 The values of drag coefficient C_D

Cases	C_D
Wave 0410, U_c=0.05 m/s	2.3
Wave 0610, U_c =0.05 m/s	2.8
Wave 0412, U_c =0.05 m/s	3.3
Wave 0612, U_c =0.05 m/s	3.7
Wave 0812, U_c =0.05 m/s	3.7
Wave 0410, U_c =0.2 m/s	1.3
Wave 0610, U_c =0.2 m/s	1.3
Wave 0412, U_c =0.2 m/s	1.4
Wave 0612, U_c =0.2 m/s	1.4
Wave 0812, U_c =0.2 m/s	1.4

The comparison of the relative wave amplitude variation in the vegetation domain is shown in **Fig. 6**. The circles, triangles, and squares represent the experimental data of incident wave height of heights of 0.04 m, 0.06 m, and 0.08 m, respectively, while the solid, dashed, and dotted lines represent that of the present model, respectively. The wave period T of **Fig. 6 (a)** and **Fig. 6 (c)** is 1.0 s, and that of **Fig. 6 (b)** and **Fig. 6 (d)** is 1.2 s. For current velocity is equal to 0.05

m/s, we can find that the larger wave attenuation rate is caused by the higher incident wave height, but for current velocity is equal to 0.2 m/s, both experimental data and the present model indicate that the incident wave height does not affect the wave attenuation rate.

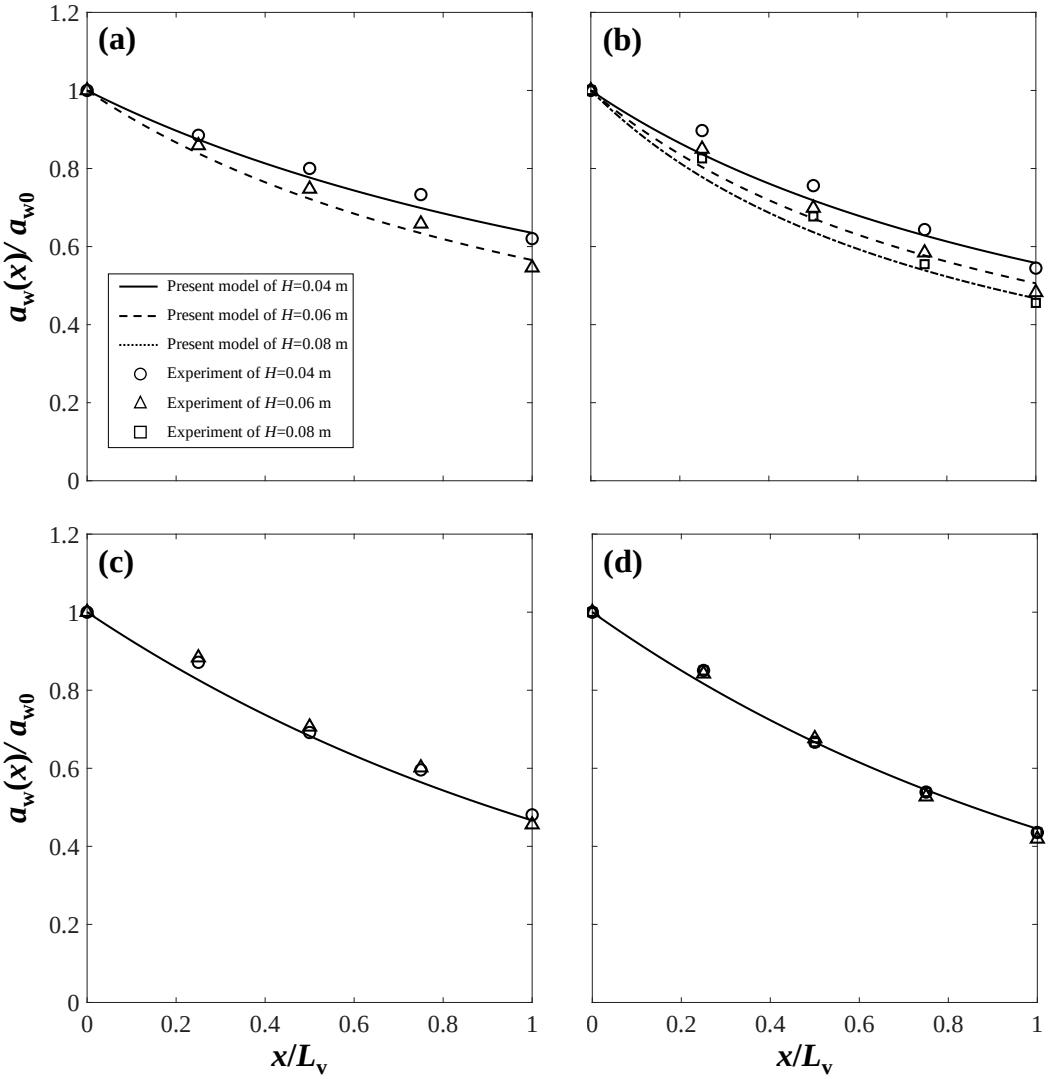

Fig. 6 Comparison of the relative wave amplitude variation of Hu et al. (2014) with present model in terms of (a) U_c=0.05 m/s, T=1.0 s, (b) U_c=0.05 m/s, T=1.2 s, (c) U_c=0.2 m/s, T=1.0 s, (d) U_c=0.2 m/s, T=1.2 s.

The velocity ratio range of the experiment is limited, therefore using the numerical model to investigate this phenomenon in a broader range of velocity ratios is necessary. The numerical experimental setup is similar to that of section 2.3. The incident wave amplitudes are added to three groups: 0.03 m, 0.04 m, and 0.05 m. The current velocity contains fourteen different velocities, which range from -0.15 m/s to 0.4 m/s. The comparison of numerical simulation with the present model is

shown in **Fig. 7**. The light blue line represents the theoretical prediction results of a_{w0}=0.05 m, the orange line represents that of a_{w0}=0.04 m, and the purple line represents that of a_{w0}=0.03 m. The black circles, triangles, and squares represent the numerical simulation results of a_{w0}=0.05 m, a_{w0}=0.04 m, and a_{w0}=0.03 m, respectively. The small image in the upper part of **Fig. 7** is an enlargement of the black dashed box area. The drag coefficient C_D is selected as 1.31 for both numerical simulation and the present model. As shown in **Fig. 7**, the numerical results agree well with the present model. The wave attenuation rate within the box is related to incident wave amplitude a_{w0} and current velocity U_c, the larger incident wave amplitude and current velocity will induce the greater wave attenuation rate. Outside the box, the wave attenuation rate is only related to current velocity U_c, and the wave attenuation rates of three different wave amplitudes will become the same.

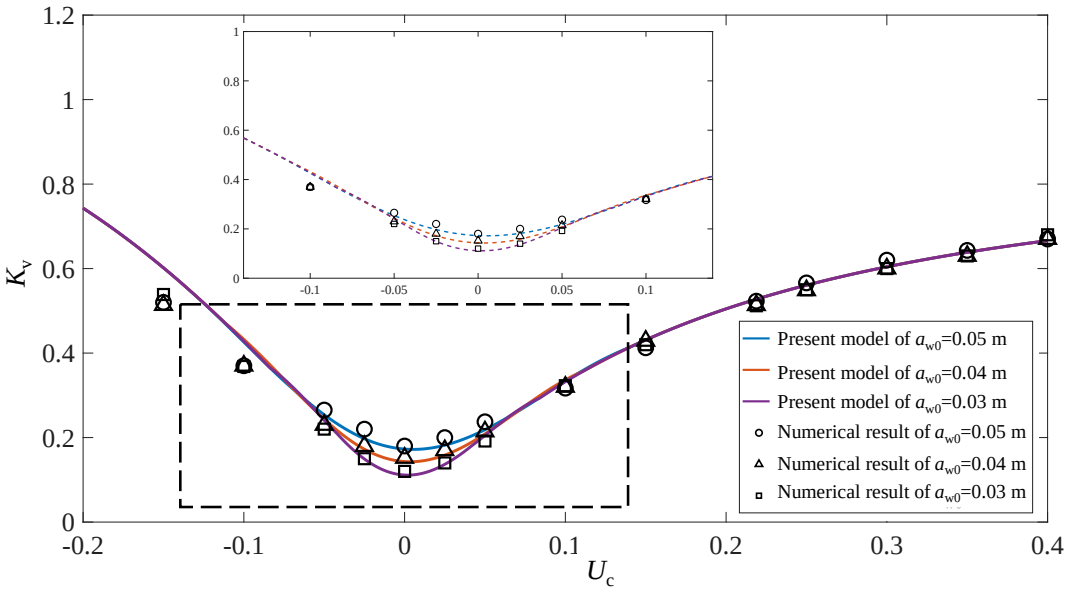

Fig. 7. The wave attenuation rate of different incident wave amplitudes and current velocities.

4. Conclusion

In this paper, we derive a new theoretical model for wave height decay in a vegetation domain by considering the ambient current of different strengths and different directions. In the derivation, the current effect on changing the wave group velocity, and thus the conservation of wave energy, is considered. To facilitate the theoretical derivation, the current strength is divided into weak, intermediate, and strong regimes, as compared to wave orbital velocity, and

different mathematical techniques are employed to arrive at the final solution. For strong current with velocity ratio $|\alpha_r| \geq 1$, we can obtain an exact solution that shows an exponential decay of wave height in vegetation domain. For weak current with $|\alpha_r| \leq \delta$, we use the Taylor expansion method at $|\alpha_r| = 0$ and obtain an asymptotic solution which shows a reciprocal decay of wave height. For current with intermediate strength, the decay pattern is the mixture of exponential decay and reciprocal decay. It is easy to prove that when current velocity U_c is equal to zero, the present model can be reduced to Dalrymple 1984 model.

Then present theory model is compared to a large amount of available experimental data and the numerical results from a RANS model that treats the vegetation domain as a special region of porous media. It is confirmed from these comparisons that the wave height decay by vegetation with the influence of current has the following interesting characteristics:

1. Due to the change of group velocity caused by current flow, for the same absolute value of current velocity, the wave decaying rate in the vegetation domain under wave opposing current conditions is greater than that under wave following current conditions.
2. With the increase of current speed, the wave height variation in the vegetation domain will change from reciprocal decay to exponential decay.
3. If the absolute value of velocity ratio α_r is less than 2/3, the wave decaying rate is related to both the incident wave amplitude a_{w0} and the current velocity U_c. The larger incident wave amplitudes will result in greater wave decaying rate. However, when the current is strong enough, i.e., the velocity ratio α_r is greater than 2/3, the wave decaying rate is independent of incident wave amplitude.

Authorship contribution statement

Huiran Liu: numerical calculation, validation, formal analysis, writing - original draft, manuscript preparation. Haiqi Fang: methodology, mathematical derivation, formal analysis, writing - review and editing. Pengzhi Lin: conceptualization, supervision.

Reference

Augustin, L.N., Irish, J.L., Lynett, P., 2009. Laboratory and numerical studies of wave damping

by emergent and near-emergent wetland vegetation. Coastal Engineering 56, 332–340. https://doi.org/10.1016/j.coastaleng.2008.09.004

Chen, M., Lou, S., Liu, S., Ma, G., Liu, H., Zhong, G., Zhang, H., 2020. Velocity and turbulence affected by submerged rigid vegetation under waves, currents and combined wave–current flows. Coastal Engineering 159, 103727. https://doi.org/10.1016/j.coastaleng.2020.103727

Dalrymple, R.A., Kirby, J.T., Hwang, P.A., 1984. Wave Diffraction Due to Areas of Energy Dissipation. Journal of Waterway, Port, Coastal, and Ocean Engineering 110, 67–79. https://doi.org/10.1061/(ASCE)0733-950X(1984)110:1(67)

Dubi, A., Tørum, A., 1995. Wave Damping by Kelp Vegetation, in: Coastal Engineering 1994. Presented at the 24th International Conference on Coastal Engineering, American Society of Civil Engineers, Kobe, Japan, pp. 142–156. https://doi.org/10.1061/9780784400890.012

Hu, Z., Lian, S., Zitman, T., Wang, H., He, Z., Wei, H., Ren, L., Uijttewaal, W., Suzuki, T., 2022. Wave breaking induced by opposing currents in submerged vegetation canopies. Water Resources Research. https://doi.org/10.1029/2021WR031121

Hu, Z., Suzuki, T., Zitman, T., Uittewaal, W., Stive, M., 2014. Laboratory study on wave dissipation by vegetation in combined current–wave flow. Coastal Engineering 88, 131–142. https://doi.org/10.1016/j.coastaleng.2014.02.009

Kobayashi, N., Raichle, A.W., Asano, T., 1993. Wave Attenuation by Vegetation. Journal of Waterway, Port, Coastal, and Ocean Engineering 119, 30–48. https://doi.org/10.1061/(ASCE)0733-950X(1993)119:1(30)

Li, C.W., Yan, K., 2007. Numerical Investigation of Wave–Current–Vegetation Interaction. J. Hydraul. Eng. 133, 794–803. https://doi.org/10.1061/(ASCE)0733-9429(2007)133:7(794)

Lin, P., 2008. Numerical modeling of water waves. CRC Press.

Lin, P., Xu, W., 2006. NEWFLUME: a numerical water flume for two-dimensional turbulent free surface flows. Journal of Hydraulic Research 44, 79–93. https://doi.org/10.1080/00221686.2006.9521663

Liu, P.L.-F., Chang, C.-W., Mei, C.C., Lomonaco, P., Martin, F.L., Maza, M., 2015. Periodic water waves through an aquatic forest. Coastal Engineering 96, 100–117. https://doi.org/10.1016/j.coastaleng.2014.11.002

López, F., García, M., 1998. open-channel flow through simulated vegetation: Suspended

sediment transport modeling. Water Resour. Res. 34, 2341–2352. https://doi.org/10.1029/98WR01922

Losada, I.J., Maza, M., Lara, J.L., 2016. A new formulation for vegetation-induced damping under combined waves and currents. Coastal Engineering 107, 1–13. https://doi.org/10.1016/j.coastaleng.2015.09.011

Lou, S., Chen, M., Ma, G., Liu, S., Zhong, G., 2018. Laboratory study of the effect of vertically varying vegetation density on waves, currents and wave-current interactions. Applied Ocean Research 79, 74–87. https://doi.org/10.1016/j.apor.2018.07.012

Ma, G., Kirby, J.T., Su, S.-F., Figlus, J., Shi, F., 2013. Numerical study of turbulence and wave damping induced by vegetation canopies. Coastal Engineering 80, 68–78. https://doi.org/10.1016/j.coastaleng.2013.05.007

Maza, M., Lara, J.L., Losada, I.J., 2015. Tsunami wave interaction with mangrove forests: A 3-D numerical approach. Coastal Engineering 98, 33–54.

Mei, C.C., Chan, I.-C., Liu, P.L.-F., Huang, Z., Zhang, W., 2011. Long waves through emergent coastal vegetation. J. Fluid Mech. 687, 461–491. https://doi.org/10.1017/jfm.2011.373

Mendez, F.J., Losada, I.J., 2004. An empirical model to estimate the propagation of random breaking and nonbreaking waves over vegetation fields. Coastal Engineering 51, 103–118. https://doi.org/10.1016/j.coastaleng.2003.11.003

Nepf, H., Ghisalberti, M., 2008. Flow and transport in channels with submerged vegetation. Acta Geophys. 56, 753–777. https://doi.org/10.2478/s11600-008-0017-y

Nepf, H.M., 1999. Drag, turbulence, and diffusion in flow through emergent vegetation. Water Resour. Res. 35, 479–489. https://doi.org/10.1029/1998WR900069

Paul, M., Bouma, T.J., Amos, C.L., 2012. Wave attenuation by submerged vegetation: combining the effect of organism traits and tidal current. Marine Ecology Progress 444, 31–41.

Pujol, D., Nepf, H., 2012. Breaker-generated turbulence in and above a seagrass meadow. Continental Shelf Research 49, 1–9. https://doi.org/10.1016/j.csr.2012.09.004

Suzuki, T., Zijlema, M., Burger, B., Meijer, M.C., Narayan, S., 2012. Wave dissipation by vegetation with layer schematization in SWAN. Coastal Engineering 59, 64–71. https://doi.org/10.1016/j.coastaleng.2011.07.006

Tang, X., Lin, P., Liu, P.L.-F., Zhang, X., 2021. Numerical and experimental studies of

596 turbulence in vegetated open-channel flows. Environ Fluid Mech 21, 1137–1163.
597 https://doi.org/10.1007/s10652-021-09812-7
598 Teh, S.Y., Koh, H.L., Liu, P.L., Ismail, A.I.Md., Lee, H.L., 2009. Analytical and numerical
599 simulation of tsunami mitigation by mangroves in Penang, Malaysia. Journal of Asian Earth
600 Sciences 36, 38–46. https://doi.org/10.1016/j.jseaes.2008.09.007
601 Yin, Z., Wang, Y., Liu, Y., Zou, W., 2020. Wave attenuation by rigid emergent vegetation under
602 combined wave and current flows. Ocean Engineering 213, 107632.
603 https://doi.org/10.1016/j.oceaneng.2020.107632
604 Zhao, C., Tang, J., Shen, Y., Wang, Y., 2021. Study on wave attenuation in following and
605 opposing currents due to rigid vegetation. Ocean Engineering 236, 109574.
606 https://doi.org/10.1016/j.oceaneng.2021.109574
607